

Inhibition of Plasma Kallikrein by a Highly Specific Active Site Blocking Antibody

Received for publication, March 27, 2014, and in revised form, June 25, 2014. Published, JBC Papers in Press, June 26, 2014, DOI 10.1074/jbc.M114.569061

Jon A. Kenniston[‡], Ryan R. Faucette[‡], Diana Martik[‡], Stephen R. Comeau[‡], Allison P. Lindberg[‡], Kris J. Kopacz[‡], Gregory P. Conley[‡], Jie Chen[‡], Malini Viswanathan[‡], Niksa Kastrapeli[‡], Janja Cosic[‡], Shauna Mason[‡], Mike DiLeo[‡], Jan Abendroth[§], Petr Kuzmic[¶], Robert C. Ladner[‡], Thomas E. Edwards[§], Christopher TenHoor[‡], Burt A. Adelman[‡], Andrew E. Nixon[‡], and Daniel J. Sexton^{‡1}

From the [‡]Dyax Corp., Burlington, Massachusetts 01803, [§]Beryllium, Bainbridge Island, Washington 98110, and [¶]Biokin, Watertown, Massachusetts 02472

Background: Unregulated plasma kallikrein proteolytic activity can result from C1-inhibitor deficiency, causing excessive and potentially fatal edema.

Results: The antibody DX-2930 potently and specifically inhibits plasma kallikrein and exhibits a long plasma half-life.

Conclusion: An antibody protease inhibitor can lead to potent and specific bioactivity.

Significance: DX-2930 could be an effective therapeutic for the prophylactic inhibition of plasma kallikrein-mediated diseases.

Plasma kallikrein (pKal) proteolytically cleaves high molecular weight kininogen to generate the potent vasodilator and the pro-inflammatory peptide, bradykinin. pKal activity is tightly regulated in healthy individuals by the serpin C1-inhibitor, but individuals with hereditary angioedema (HAE) are deficient in C1-inhibitor and consequently exhibit excessive bradykinin generation that in turn causes debilitating and potentially fatal swelling attacks. To develop a potential therapeutic agent for HAE and other pKal-mediated disorders, we used phage display to discover a fully human IgG1 monoclonal antibody (DX-2930) against pKal. *In vitro* experiments demonstrated that DX-2930 potently inhibits active pKal ($K_i = 0.120 \pm 0.005$ nM) but does not target either the zymogen (prekallikrein) or any other serine protease tested. These findings are supported by a 2.1-Å resolution crystal structure of pKal complexed to a DX-2930 Fab construct, which establishes that the pKal active site is fully occluded by the antibody. DX-2930 injected subcutaneously into cynomolgus monkeys exhibited a long half-life ($t_{1/2} \sim 12.5$ days) and blocked high molecular weight kininogen proteolysis in activated plasma in a dose- and time-dependent manner. Furthermore, subcutaneous DX-2930 reduced carrageenan-induced paw edema in rats. A potent and long acting inhibitor of pKal activity could be an effective treatment option for pKal-mediated diseases, such as HAE.

The plasma contact system is driven by the coordinated action of coagulation factor XII (FXII),² pKal, and HMWK to

generate proteolytically activated mediators of vascular biology, thrombosis, fibrinolysis, angiogenesis, and inflammation (1). Positioned at the interface between coagulation and inflammation, the contact system initiates intrinsic pathway coagulation and activates the plasma kallikrein-kinin system (KKS) by conversion of prekallikrein to active pKal. pKal is a serine protease that cleaves HMWK at two sites to liberate bradykinin, a nonapeptide agonist of the constitutive bradykinin B2 G-protein-coupled receptor and via its des-Arg⁹ bradykinin metabolite, an agonist of the inducible bradykinin B1 G-protein-coupled receptor (Fig. 1) (2). Activation of these receptors leads to the production of mediators of inflammation, vasodilation, angiogenesis, and pain (2).

Pathophysiologic *in vivo* triggers of contact system activation in human disease have been difficult to identify. However, the system has been shown to be activated *in vitro* and in preclinical disease models by numerous agents that include mast cell heparin (3), misfolded or aggregated proteins (4), sub-endothelial matrix proteins such as collagens and laminin (5–7), extracellular RNA (8), polyphosphate from platelets or bacteria (9, 10), fibrin (11), bacterial infection (12), ventricular assist devices (13), and following exposure of plasma to polyanionic substances such as kaolin, dextran sulfate, phospholipids, or surfaces such as glass (1). Furthermore, there are reports that the contact system is activated in plasma obtained from patients with diseases such as rheumatoid, psoriatic, or osteoarthritis (14), ulcerative colitis (15), systemic lupus erythematosus (16), psoriasis (16), diabetic retinopathy, and macular edema (17, 18), sepsis (19), systemic amyloidosis (4), sickle cell disease (20), Alzheimer disease (21), anaphylaxis (3), brain ischemia and edema (22), cirrhosis (23), and hereditary angioedema with C1-inhibitor deficiency (HAE-C1INH) (24–26).

⌘ Author's Choice—Final version full access.

The atomic coordinates and structure factors (codes 4OGY, 4OGX, and 4PUB) have been deposited in the Protein Data Bank (<http://www.pdb.org/>).

¹ To whom correspondence should be addressed: Dyax Corp., 55 Network Drive, Burlington, MA 01803-2756. Tel.: 617-250-5784; Fax: 617-225-2501; E-mail: dsexton@dyax.com.

² The abbreviations used are: FXII, factor XII; AEBSF, 4-(2-aminoethyl) benzenesulfonyl fluoride hydrochloride; C1-INH, C1 inhibitor; CDR, complementarity determining region; CPE, carrageenan-induced paw edema; Fab, fragment antigen binding domain; FXIIa, activated FXII; HAE-C1INH, hereditary angioedema with C1-inhibitor deficiency; HMWK, high molecular

weight kininogen; HV, antibody heavy chain variable domain; LV, antibody light chain variable domain; KKS, plasma kallikrein-kinin system; pKal, activated plasma kallikrein; SPR, surface plasmon resonance; cv, column volume; PDB, Protein Data Bank; r.m.s.d., root mean square deviation; AMC, amido-4-methylcoumarin; RU, response unit; Z, benzyloxycarbonyl; CDR, complementary determining region; FR, framework.

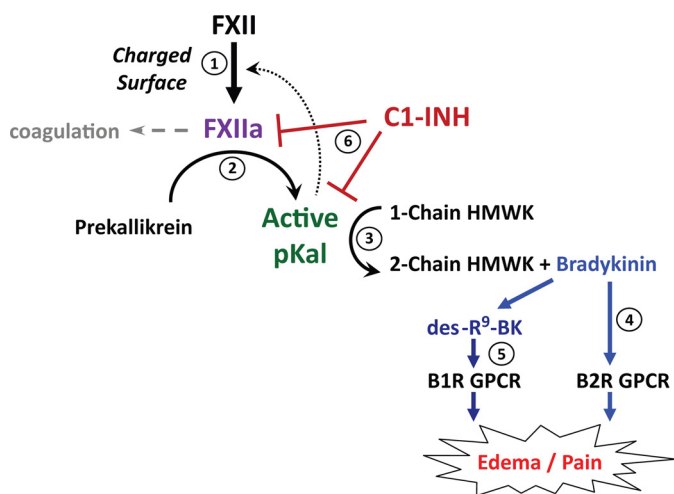


FIGURE 1. Activation cycle of the kallikrein-kinin enzymatic pathway. Autoactivation of the proenzyme form of factor XII to XIIa (step 1) initiates a proteolytic cascade that activates pKal (step 2), which in turn cleaves HWMK to release bradykinin (step 3) (in addition to the positive feedback activation of more FXII). Bradykinin subsequently binds and activates the bradykinin B₂ receptor (step 4), thereby initiating an intracellular signaling cascade that ultimately results in swelling and pain in the affected tissues. Exoprotease activity on bradykinin generates des-Arg⁹bradykinin, which signals through the bradykinin B₁ receptor (step 5). Individuals with HAE are deficient in C1-INH (step 6), the major inhibitor of active pKal and FXIIa, and subsequently exhibit unpredictable attacks of bradykinin-mediated pain and edema.

HAE-C1INH is a rare disease caused by unregulated activation of the KKS that clinically manifests as intermittent attacks of subcutaneous or mucosal edema affecting the face, larynx, gastrointestinal tract, limbs, or genitalia (27). Affected individuals harbor autosomal dominant mutations in the C1-INH gene (SERPING1) that lead to a deficiency in either total (type I HAE-C1INH) or functional (type II HAE-C1INH) C1-INH protein, a protease inhibitor of the serpin superfamily that regulates the contact, coagulation, fibrinolytic, and complement pathways (28, 29). During an HAE attack, reduced levels of functional C1-INH are insufficient to inhibit its key targets, both FXIIa and pKal (Fig. 1), thereby causing the overproduction of bradykinin and ultimately the pain and swelling characteristic of this disease.

Clinically, the role of the plasma KKS in HAE-C1INH pathophysiology has been demonstrated by the approval of therapeutics that inhibit this pathway. For treatment of acute attacks, these include C1-INH replacement, selective inhibition of pKal proteolytic activity with the Kunitz domain inhibitor ecallantide, or bradykinin B₂ receptor antagonism with the bradykinin peptidomimetic icatibant (30). Prophylactic treatments include chronic C1-INH replacement, which is limited by the need for frequent intravenous administration that can lead to the placement of an indwelling catheter. C1-INH therapy is also associated with a risk for serious thromboembolic events (31). Oral androgens are an alternative prophylactic option that are more convenient to administer but are associated with serious toxicities and morbidities from unwanted androgenizing effects, particularly in women, as well as hepatic adenomas with malignant potential (32, 33). Furthermore, despite chronic treatment with existing prophylactic agents, breakthrough attacks still occur (34). Thus, there remains an unmet medical need for a

long lasting, convenient, safe, and effective prophylactic therapeutic to treat HAE-C1INH.

Given the potential for target specificity and long serum half-life with antibody therapeutics, we used phage display to select a potent and highly specific human antibody inhibitor of pKal, DX-2930. Here, we describe the discovery and biochemical characterization of DX-2930, including the x-ray structure of the Fab·pKal complex, which provides a rationale for the specificity and effectiveness of DX-2930. Moreover, preclinical studies reveal DX-2930 to exhibit a prolonged half-life in circulation, and we further demonstrate that this translates into a prolonged capacity to inhibit the KKS. Taken together, data presented here support the potential of DX-2930 for the prophylactic inhibition of pKal-mediated edema and provide a highly specific reagent tool to investigate the effects of targeted pKal inhibition in complex biological samples containing highly homologous proteases.

EXPERIMENTAL PROCEDURES

Proteins—Full-length human plasma kallikrein (prekallikrein and activated pKal forms), 1-chain kininogen (intact kininogen), and 2-chain kininogen (treated with pKal to excise bradykinin) were obtained from Enzyme Research Laboratories. C1-INH and pKal orthologues from rat, cynomolgus monkey, and rabbit plasma were purified by Athens Research and Technology. The pKal catalytic domain variant used in crystallographic studies contained three deglycosylation (N396E, N453E, and N494E) and two cysteine (C383S and C503S) mutations and were purified as described previously (35).

Specificity—DX-2930 specificity screen measurements used the following 20 human serine proteases. Recombinant complement component C1s (R & D Systems) was assayed using 10 μ M dabcyL-Ser-Leu-Gly-Arg-Lys-Ile-Gln-Ile-EDANS (where dabcyL is 4-((4-(dimethylamino)phenyl)azo)benzoyl and EDANS is 5-[(2-aminoethyl)amino]naphthalene-1-sulfonic acid) as substrate in Buffer A (25 mM Tris, pH 8.0, 100 mM NaCl, 0.01% Brij35). Factor XIIa (Enzyme Research Labs) was assayed using 10 μ M Pro-Phe-Arg-AMC (where AMC is 7-amino-4-methylcoumarin) as substrate in Buffer B (20 mM Tris-HCl, pH 7.5, 150 mM NaCl, 1 mM EDTA, 0.1% PEG-8000, and 0.1% Triton X-100). Activated protein C (Haematologic Technologies, Inc.) was assayed using 50 μ M Boc-D-VLR-ANSNH-C4H9 (where ANSNH is 6-amino-1-naphthalene-sulfonamide) as substrate in Buffer C (100 mM Tris-HCl, pH 8.0, 50 mM NaCl, 10 mM CaCl₂, 0.025% CHAPS). Cathepsin G (Biomol) was assayed using 10 μ M succinyl-Ala-Ala-Pro-Phe-AMC as substrate in Buffer C. Factor VIIa (Biomol) was assayed using 10 μ M Z-Val-Val-Arg-AMC as substrate in Buffer A. Factor Xa (Biomol) was assayed using 10 μ M CH₃SO₂-D-CHA-Gly-Arg-AMC-AcOH as substrate in Buffer A containing 0.25 mg/ml bovine serum albumin (BSA). Factor XIa (Haematologic Technology Inc.) was assayed using 10 μ M *t*-butyloxycarbonyl-Glu(benzyl ester)-Ala-Arg-MCA (where MCA is 4-methylcoumarinyl-7-amide) as substrate in Buffer A. Recombinant granzyme B (Biomol) was assayed using 10 μ M Ac-Ile-Glu-Pro-Asp-AMC as substrate in Buffer A. Recombinant hepsin (R & D Systems) was assayed using 10 μ M Pro-Phe-Arg-AMC as substrate in Buffer B. Recombinant matriptase (R & D Systems) was assayed using 10

Antibody Inhibition of Plasma Kallikrein

μM Pro-Phe-Arg-AMC as substrate in Buffer B. Neutrophil elastase (Athens Research and Technology) was assayed using $100 \mu\text{M}$ *N*-methoxysuccinyl-Ala-Ala-Pro-Val-AMC as substrate in Buffer B. Plasmin (Haematologic Technology Inc.) was assayed using $10 \mu\text{M}$ H-D-CHA-Ala-Arg-AMC as substrate in Buffer A. Thrombin α (Enzyme Research Labs) was assayed using $10 \mu\text{M}$ H-D-CHA-Ala-Arg-AMC as substrate in Buffer A containing 2.5 mM CaCl_2 and 1 mg/ml BSA. Recombinant tissue kallikrein 1 (R & D Systems) was assayed using $10 \mu\text{M}$ Pro-Phe-Arg-AMC as substrate in Buffer B. Recombinant tissue kallikrein 2 (36) was assayed using $10 \mu\text{M}$ Pro-Phe-Arg-AMC as substrate in Buffer B. Recombinant tissue kallikrein 5 (R & D Systems) was assayed using $10 \mu\text{M}$ Z-Val-Val-Arg-AMC as substrate in Buffer A. Recombinant tissue kallikrein 12 (R & D Systems) was assayed using $10 \mu\text{M}$ Val-Pro-Arg-AMC as substrate in Buffer C. Trypsin (Athens Research and Technology) was assayed using $10 \mu\text{M}$ Pro-Phe-Arg-AMC as substrate in Buffer B. Recombinant tissue plasminogen activator (Sigma) was assayed using $10 \mu\text{M}$ Z-Gly-Pro-Arg-AMC as substrate in Buffer A containing 1% BSA. Urokinase (Sigma) was assayed using $10 \mu\text{M}$ benzyl-Ala-Gly-Arg-AMC as substrate in Buffer A.

Phage Display Selection and Primary Screening—Human antibodies against pKal were obtained by panning an antibody phage display library (37) against biotinylated pKal immobilized on streptavidin-coated magnetic beads (Dyna, M280). Selections were performed as described (38), including positive selections with decreasing amounts of biotinylated human or rat pKal and negative selections with untreated streptavidin beads and biotinylated prekallikrein. Phage isolates were screened by ELISA (streptavidin-immobilized pKal with detection by anti-M13 coat protein VIII), positive hits were DNA-sequenced, and unique Fabs were batch-processed for *Escherichia coli* expression as isolated Fab fragments from the pMID21 vector as described (38). An affinity maturation library was constructed around the lead Fab (given its inhibition of both human and rat pKal) by employing mixed nucleotide synthesis of heavy chain variable complementary determining region 3 (HV-CDR3) where the nominal base was present at 85% and each of the others at 5% .

Antibody Expression and Purification—High throughput production of *E. coli*-secreted Fabs and their subsequent purification by protein A-Sepharose followed previously reported protocols (38). The DX-2930 Fab construct generated for crystallization studies was produced as follows. The DNA sequence for the DX-2930 Fab region was codon-optimized and cloned into the pJexpress 401 expression vector by DNA2.0. SS320 TG1 *E. coli* cells (Lucigen) were transformed with the Fab expression vector and grown in 10 ml of TBDry media containing 2% glucose and $25 \mu\text{g/ml}$ kanamycin for 18 h at 30°C . 10 liters of TBDry media containing 0.1% glucose and $25 \mu\text{g/ml}$ kanamycin was then inoculated with 10 ml of the starter culture ($1:1000$ ratio) and grown for 20 h at 30°C . Cells were harvested by centrifugation (15 min at $2000 \times g$); the pellet resuspended in 10 liters with TBDry media containing $25 \mu\text{g/ml}$ kanamycin, 1 mM isopropyl 1-thio- β -D-galactopyranoside, and 0.5% Triton X-100, and incubated an additional 20 h at 30°C with shaking. The culture was finally harvested by spinning at $9000 \times g$ for 30 min and filtered through a Corning $0.22\text{-}\mu\text{m}$ PES filter. The

resulting culture supernatant containing secreted Fab protein was subjected to a three-step chromatography purification. Fab product was first captured by immunoaffinity protein A resin (RepliGen). 80 ml of immobilized protein A resin was added to the 10 liters of filtered supernatant and incubated with rocking for 18 h at 4°C . Resin was captured in a fritted column and extensively washed to remove host cell-related impurities and reduce endotoxin level. Washes successively included 10 column volumes (cv) of PBS, 20 cv of Fab Wash Buffer (50 mM sodium acetate, 0.5 M sodium chloride, $\text{pH } 5.0$), 50 cv of PBS with 0.1% Triton X-100, and then a final wash with 50 cv PBS. Soluble Fab (sFab) was then eluted from protein A with 6 cv of Fab elution buffer (50 mM sodium phosphate, 150 mM sodium chloride, $\text{pH } 2.5$) and instantly neutralized to $\text{pH } 6.0$ with 2 cv equivalents of 1 M HEPES, $\text{pH } 7.2$. Neutralized protein A eluate was loaded onto PBS pre-equilibrated mercaptoethylpyridine HyperCel resin (Pall Lifesciences) and incubated overnight at 4°C with rocking. Mercaptoethylpyridine resin was then washed with 10 cv of PBS, followed by step elutions with 50 mM sodium acetate solutions at varying pH values from $\text{pH } 5$ to $\text{pH } 3$. The major elution peak at $\text{pH } 5$ was collected and directly loaded onto a POROS HS 50 strong CEX resin (Invitrogen) pre-equilibrated with 50 mM sodium acetate, $\text{pH } 4.5$ (“CEX Buffer”), washed first with the same CEX Buffer, and then an additional wash with CEX Buffer + 250 mM NaCl. Fab was subsequently eluted with CEX Buffer + 350 mM NaCl. Purified Fab product was exchanged into a buffer containing 50 mM citrate/phosphate, 100 mM NaCl, $\text{pH } 6.0$, through an ultrafiltration/diafiltration process using a Millipore Amicon Ultra concentration unit ($10,000\text{-kDa}$ molecular mass cutoff). Recombinant Fab fragments were reformatted into full-length human IgG1 antibodies (f-allotype) (39), expressed as stable transfections in CHO cells using a fed-batch fermentation strategy, and purified as previously described (40) into formulation buffer (100 mM citrate/phosphate buffer, $\text{pH } 6.0$, 50 mM NaCl, 2% (w/v) trehalose, and 0.01% Tween 80).

Enzyme Inhibition Analysis—Steady state inhibition measurements were performed as described previously (40). Briefly, pKal (nominal concentration of 1 nM as total protein) was incubated with different concentrations of inhibitor for 1 h at 30°C in Buffer B (20 mM Tris-HCl, $\text{pH } 7.5$, 150 mM NaCl, 1 mM EDTA, 0.1% PEG-8000, and 0.1% Triton X-100) in a 96-well plate. The maximum final inhibitor concentration was 10 nM , followed by a 1.5-fold serial dilution (total 11 nonzero inhibitor concentrations) plus a control ($[I]_0 = 0$). The reactions were initiated by the addition of H-Pro-Phe-Arg-AMC substrate (Sigma, catalogue no. P9273) at a final concentration of 10 , 50 , or $100 \mu\text{M}$ and monitored in a fluorescence plate reader (SpectraMax, Molecular Devices) with excitation and emission wavelengths at 360 and 480 nm , respectively. Initial reaction rates were determined by linear fit of raw experimental data traces (fluorescence *versus* time) as the slopes of the regression lines. The initial reaction rates, v , were fit to Equation 1.

$$v = A \frac{[E]_0 - [I]_0 - K_i^{\text{app}} + \sqrt{([E]_0 - [I]_0 - K_i^{\text{app}})^2 + 4[E]_0 K_i^{\text{app}}}}{2}$$

(Eq. 1)

In Equation 1, $[I]_0$ is the inhibitor concentration; $[E]_0$ is the active enzyme concentration; K_i^{app} is the apparent inhibition constant; and A is an empirical constant equal to $\epsilon_p k_{\text{cat}} [S]_0 / ([S]_0 + K_m)$, where ϵ_p is the molar response coefficient of the reaction product; k_{cat} is the turnover number; $[S]_0$ is the initial substrate concentration; and K_m is the Michaelis constant. The adjustable parameters were A , K_i^{app} , and $[E]_0$. Note that Equation 1 is Cha's variant (see Equation 14 in Ref. 41) of the rate equation initially derived by Morrison (42). In contrast with Morrison's original formulation, the enzyme concentration $[E]_0$ does not appear in the denominator and instead is subsumed in the empirical constant A . This formulation significantly increases numerical stability in nonlinear regression for the following reason. In our particular case ($[E]_0 = 1 \text{ nM}$, $K_i^{\text{app}} \approx 0.1 \text{ nM}$) the enzyme concentration $[E]_0$ must be treated as an adjustable parameter, according to the theoretical principles explained elsewhere (43). However, during the iterative regression analysis, $[E]_0$ could transiently attain values very near zero, which could cause numerical underflow ("division by zero") in the original form of the Morrison equation (42). The Michaelis constant K_m for the synthetic substrate was determined to be $315 \pm 16 \mu\text{M}$ (data not shown). At a substrate concentration $[S]_0 = 10 \mu\text{M}$, the factor $1 + [S]_0/K_m$ in Equation 2 (assuming competitive inhibition, see *inset* in Fig. 2A) is equal to 1.03.

$$K_i^{\text{app}} = K_i (1 + [S]_0/K_m) \quad (\text{Eq. 2})$$

Thus, in our particular case the apparent inhibition constants K_i^{app} obtained in the regression analysis are identical to the true inhibition constant within 3%. The activity of 20 different human serine proteases listed above was observed in the absence or presence of $1 \mu\text{M}$ DX-2930 using synthetic chromogenic or fluorogenic substrates.

ELISA Measurement of pKal-mediated Bradykinin Formation—Following the incubation of human pKal (0.15 nM) with varying concentrations of DX-2930 for 1 h at 30 °C in Buffer B, 1-chain HMWK was added at a final concentration of 20 nM. After the reaction proceeded for 10 min at 30 °C, samples were applied to a 96-well 10-kDa molecular mass cutoff filter plate (Millipore MultiScreen with Ultracel-10 membrane), centrifuged at $400 \times g$ in a table top centrifuge for 45 min to remove unreacted HMWK, and analyzed by an anti-bradykinin ELISA (Peninsula Laboratories) per the manufacturer's instructions.

ELISA Detection of pKal Binding to HUVEC—Human umbilical vein endothelial cells (Lonza) were seeded onto 96-well plates at $\sim 2 \times 10^4$ cells/well, and incubated for 48 h. The wells were blocked with 3% BSA in Buffer D (20 mM HEPES, 150 mM NaCl, 2 mM CaCl_2 , 1 mM MgCl_2 , pH 7.5), washed, and then treated with Buffer E (Buffer D + 50 μM ZnSO_4 and 0.5 mg/ml BSA) or HMWK (40 nM in Buffer E) for 1 h at 25 °C, followed by a 1-h incubation with 3 nM pKal or pKal pretreated with 1 mM 4-(2-aminoethyl) benzenesulfonyl fluoride hydrochloride (AEBSF, Thermoscientific). Varying concentrations of biotinylated DX-2930 were then added to the treated cells for 2 h, and bound antibody was detected by streptavidin-alkaline phosphatase and *p*-nitrophenyl phosphate additions.

Surface Plasmon Resonance—Surface plasmon resonance (SPR) measurements were performed using a BIAcore 3000 (GE Healthcare) with the detection temperature at 25 °C and HBS-P running buffer (10 mM HEPES, pH 7.4, 150 mM NaCl, and 0.005% surfactant P20). To measure kallikrein interactions with DX-2930, goat anti-human Fc fragment-specific IgG (Jackson ImmunoResearch) was immobilized by amine coupling on a CM5 sensor chip at ~ 5000 response units (RU), and DX-2930 was subsequently captured by injecting a 5 nM antibody solution for 4 min at 5 $\mu\text{l}/\text{min}$. Reference surfaces were activated and blocked in mock amine coupling reactions. 500 nM prekallikrein, pKal, or pKal-AEBSF were injected for 5 min at 20 $\mu\text{l}/\text{min}$ followed by a 5-min dissociation phase. Surfaces were regenerated with a 30-s pulse of 10 mM glycine, pH 1.5, at 100 $\mu\text{l}/\text{min}$. To measure the affinity of pKal to HMWK, 2-chain HMWK was immobilized by amine coupling on a CM5 chip at ~ 2000 RU, and varying concentrations of pKal were flowed over the surface for 5 min at 20 $\mu\text{l}/\text{min}$, and dissociation followed for 5 min. Equilibrium RU values for each pKal concentration, $[E]$, were fit to Equation 3 to obtain the observed dissociation equilibrium constant K_D . Reference surface and chip regeneration followed the above procedures.

$$\text{RU} = \text{RU}^{\text{max}} \frac{[E]}{[E] + K_D} \quad (\text{Eq. 3})$$

X-ray Crystallographic Structure of the DX-2930-pKal Complex—Purified DX-2930 Fab and the deglycosylated pKal catalytic domain variant (35) were incubated at 1:1 stoichiometry. The resulting complex (150 μM) in addition to Fab alone was diluted 1:1 in reservoir precipitant (Table 2) and crystallized by the hanging drop vapor diffusion method. Diffraction data from resulting crystals were collected with a Rigaku FR-E+ Super-Bright x-ray generator with a Saturn 944+ CCD detector and VariMax HF optics (complex) and at the Argonne National Laboratory (APS) beam line (Fab alone, refer to Table 2). The complex structure was solved by molecular replacement in Phaser using separate constant and variable domains of a Fab model (derived from PDB 3IDX) and the pKal catalytic domain structure PDB 2ANY (35). The crystallographic model of the 2930 Fab determined from the pKal:2930 Fab complex structure was then used to help solve the Fab-only structure. The final models were obtained after iterative building/refinement in REFMAC/COOT (44–46).

Pharmacokinetic Properties of DX-2930 in Cynomolgus Monkey—Six male cynomolgus monkeys were assigned to two dose groups, each consisting of three animals. All animals (treated at WIL Research) were dosed on day 0, with group 1 receiving a single i.v. injection of 20 mg/kg DX-2930 (2 ml/kg of DX-2930 at 10 mg/ml) and Group 2 receiving a single s.c. injection of 20 mg/kg DX-2930 (also 2 ml/kg of DX-2930 at 10 mg/ml). Blood was collected from all animals in citrated plastic tubes at the following time points: predose, 5 min; 1, 4, 24, 48, 96, 168, 240, 336, 432, 504, 672, 840, and 1008 h post-dose. Plasma samples were analyzed using a qualified sandwich ELISA method. Briefly, 96-well microplates (Costar 3059) were coated with 1 $\mu\text{g}/\text{ml}$ goat anti-human IgG (Bethyl Labs: preadsorbed with monkey IgG; diluted in 100 mM sodium carbon-

Antibody Inhibition of Plasma Kallikrein

ate, pH 9.4) by incubation at 4 °C overnight and subsequently blocked with 3% BSA in 1× PBS (incubated 2 h at 37 °C). Test sample and antibody standards were then diluted 1:10 with PBST-B (1× PBS, 0.1% Tween 20, and 3% BSA) and captured on the microplate by incubation for 2 h at 37 °C. Finally, bound IgG/DX-2930 was detected by the addition of 50 ng/ml HRP-labeled goat anti-human IgG (Bethyl Labs) diluted in PBST-B. Antibody standard dilutions were included to calculate the concentration of DX-2930 in sample plasma. From these data, the pharmacokinetic parameters were calculated using WinNonlin Professional Version 5.3 (Pharsight Inc.). All data were analyzed noncompartmentally.

Ex Vivo Analysis of HMWK Cleavage by pKal—Cynomolgus monkeys were subcutaneously injected with 25 and 50 mg/kg DX-2930, and blood was collected as above at WIL Research. Aliquots of the resulting citrated plasma samples were activated with 150 μg/ml kaolin for 10 min at 37 °C, diluted 1:20 in 1× PBS, and aliquots analyzed by Western blots blocked in PBST + 2% BSA and probed with 1:2000 HRP-labeled sheep anti-human kininogen polyclonal antibody (Cedarlane) diluted in PBST + 2% BSA.

Carrageenan-induced Paw Edema—Male Sprague-Dawley rats (180–200 g each, Harlan Laboratories) were divided into different treatment groups ($n = 10$ each group) and treated at Washington Biotechnology, Inc., with either an i.p. injection of Formulation Buffer, indomethacin-positive control (Sigma, 5 mg/kg prepared in 0.1 M NaHCO₃ at a concentration of 2.5 mg/ml), or an s.c. injection of different doses of DX-2930. The i.p. and s.c. injections were administered 30 min and 24 h, respectively, prior to the injection of 0.1 ml of 1% λ carrageenan (FLUKA, prepared in distilled water) into the right hind paw. Paw volumes were measured by plethysmography before and 1, 2, 4, 6, and 8 h after carrageenan injection.

RESULTS

Discovery of DX-2930 by Antibody Phage Display and Affinity Maturation—Phage isolates were screened for interaction with pKal by ELISA, and hits were characterized using purified Fab fragments. Of these, one Fab (M0162-A04) was selected for affinity maturation given that it inhibited the proteolytic activity of both human and rat pKal with equal potency ($K_i^{app} \approx 5$ nM), while not binding prekallikrein (data not shown). A comparison of apparent inhibition constants (K_i^{app}) and HV-CDR3 amino acid sequences for the most potent inhibitors obtained from the affinity maturation campaign (Table 1) revealed that only a few amino acid substitutions were necessary to significantly improve potency. For instance, the introduction of a valine at position 5 (I103V) in HV-CDR3 alone improved the affinity almost 10-fold (e.g. the M0201-H06 Fab, $K_i^{app} = 0.56$ nM), although the combination of T101I and A108E substitutions along with I103V (isolate M0199-A08) further improved the potency toward pKal ($K_i^{app} = 0.05$ nM). Including rational mutagenesis (Table 1) and consideration of invariant residues post affinity maturation (e.g. Pro-104 and Arg-105), a common motif for the HV-CDR3 interaction with pKal is evident (shown as a modified SeqLogo in Table 1). Ultimately, the M0199-A08 variant was chosen to be reformatted for production as a germ line-optimized human IgG1 in CHO cells given its favorable

TABLE 1
Summary of HV-CDR3 affinity maturation

| Initial Name | HV CDR3 | K_i^{app} (nM) ^a |
|--------------|----------------|-------------------------------|
| M0162-A04 | RRTGIPRRDAFDI | 5.39 ± 0.50 |
| M0199-A11 | --R----- | 2.00 ± 0.23 |
| M0201-F11 | --S----- | 2.95 ± 0.35 |
| M0202-A08 | -----W---- | 2.72 ± 0.31 |
| M0201-A06 | -----V---- | 3.75 ± 0.35 |
| M0202-E03 | -----E- | 2.12 ± 0.36 |
| M0199-B01 | -----N | 1.55 ± 0.14 |
| M0200-B01 | -----S | 3.59 ± 0.37 |
| M0201-H06 | ----V----- | 0.56 ± 0.04 |
| M0202-H05 | ----V----V--- | 0.24 ± 0.04 |
| M0201-H08 | ----V-----L-N | 0.80 ± 0.13 |
| M0200-E11 | ----V-----N | 0.38 ± 0.04 |
| M0200-H07 | ----V---N---N | 0.42 ± 0.03 |
| M0202-F06 | ----V--W----- | 0.33 ± 0.02 |
| M0200-A10 | ----V----S--- | 0.23 ± 0.03 |
| M0202-G03 | ----V----S-E- | 0.33 ± 0.02 |
| M0202-A12 | Q---V----S-N- | 0.09 ± 0.01 |
| M0202-H03 | ----V--W-D--- | 0.03 ± 0.01 |
| M0201-A07 | ----V-----E--- | 0.12 ± 0.02 |
| M0202-C02 | --P-V----- | 0.55 ± 0.05 |
| M0202-B04 | --S-V----- | 0.18 ± 0.01 |
| M0202-E06 | --R-V----D--- | 0.05 ± 0.01 |
| M0202-A01 | --I-V----- | 0.30 ± 0.02 |
| M0202-D09 | --I-V----S--- | 0.17 ± 0.01 |
| M0200-D03 | --I-V----S--M | 0.09 ± 0.01 |
| M0202-C09 | --I-V----D--- | 0.05 ± 0.01 |
| M0199-A08 | --I-V----E--- | 0.05 ± 0.01 |
| Mutant 1 | --I----- | 1.75 ± 0.18 |
| Mutant 2 | --I-----E--- | 0.26 ± 0.02 |
| Mutant 3 | ----A----- | 228 ± 19 |
| Mutant 4 | ----S----- | 913 ± 274 |
| Mutant 5 | ----L----- | 12.6 ± 1.08 |
| Mutant 6 | -----E--- | 2.92 ± 0.48 |

Position^b



^a K_i^{app} determined for full-length pKal by potency studies like those shown in Fig. 2A.

^b Residue positions were specific for DX-2930. Sequence logo is shown for the affinity maturation output and weighting isolates for their capacity to inhibit pKal (higher weight to lower K_i).

potency, specificity, and protein expression/stability properties, and it is hereafter referred to as DX-2930.

DX-2930 Is a Potent Inhibitor of pKal—DX-2930 retains its potent *in vitro* inhibition of pKal as a full-length human IgG1 (Fig. 2A). The observed linear increase in K_i^{app} values with increasing substrate concentrations is consistent with a competitive inhibition mechanism for DX-2930 (Fig. 2A, inset).

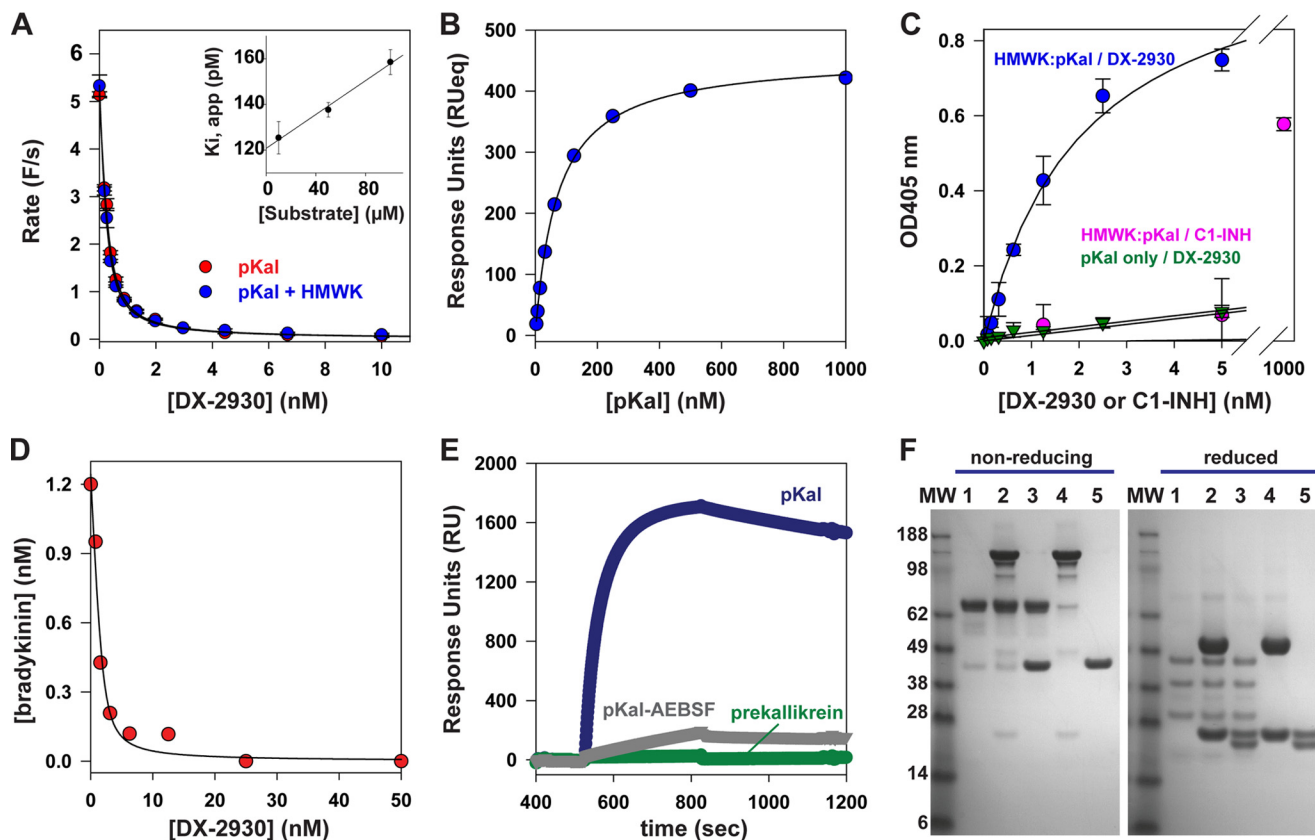


FIGURE 2. DX-2930 potently inhibits pKal proteolytic activity. *A*, increasing concentrations of DX-2930 were incubated with full-length pKal until equilibrium was achieved, and the rate of pKal-mediated proteolysis of the peptide PFR-AMC was measured by fluorescence changes over time (F/s). Inhibition data were fit to Equation 1. The inset demonstrates the linear increase in K_i^{app} for DX-2930 interaction with pKal alone as a function of increasing substrate concentration. This behavior is consistent with a competitive inhibition mechanism (41), yielding an average $K_i = 0.120 \pm 0.005$ nM from Equation 2 (see under "Experimental Procedures"). A similar K_i value was generated for pKal that was preincubated with 600 nM HMWK (e.g., $K_i = 0.115 \pm 0.003$ nM), an excess concentration of HMWK that promotes near-complete complex formation with pKal as shown in *B*, a plot of equilibrium biosensor response units (RU) with increasing concentrations of pKal flowed over a biosensor surface bearing immobilized HMWK. *C*, ELISA detection of DX-2930 binding to pKal complexed with HMWK that is HUVEC cell membrane-bound. Unlike C1-INH, DX-2930 can effectively target membrane-anchored pKal. *D*, DX-2930 also potently inhibits cleavage of the native pKal substrate HMWK and consequently prevents the release of detectable bradykinin, as assessed by a semi-quantitative ELISA that detects the bradykinin nonapeptide in solution. Error bars shown above are the standard deviation between replicates. *E*, characterization of DX-2930 binding specificity by surface plasmon resonance. The binding of 500 nM pKal, prekallikrein, and pKal-AEBSF to a DX-2930-coated biosensor surface was monitored over time. The loss of binding to both the prekallikrein and pKal-AEBSF samples suggests DX-2930 interacts with the pKal active site. *F*, Coomassie-stained SDS-PAGE analysis of DX-2930 IgG or Fab construct (both at 2 μ M) incubated with 2 μ M pKal for 30 min at 30 °C. No proteolysis of DX-2930 IgG or Fab is observed in either reducing (5 mM DTT) or nonreducing PAGE (no new fragments generated), confirming that the intimate binding of the DX-2930 HV-CDR3 loop with the pKal active site does not result in cleavage of the antibody. Lane 1, pKal only; lane 2, pKal and DX-2930; lane 3, pKal and DX-2930 Fab; lane 4, DX-2930 only; lane 5, DX-2930 Fab only.

Using Equation 2, the inhibition constant K_i was calculated at each substrate concentration and averaged ($K_i = 0.120 \pm 0.005$ nM) (Fig. 2A). DX-2930 also inhibited purified pKal from mouse ($K_i^{app} = 0.17$ nM), rat ($K_i^{app} = 0.17$ nM), rabbit ($K_i^{app} = 14.2$ nM), and cynomolgus monkey ($K_i^{app} = 0.07$ nM) (data not shown).

In plasma, a major fraction of circulating pKal is bound to HMWK via sites distal from both the pKal catalytic domain and the bradykinin-containing domain of HMWK (1). Therefore, we also tested whether DX-2930 inhibits pKal complexed with 2-chain HMWK, a form of HMWK that lacks bradykinin (Fig. 2A). The observed dissociation constant (K_D) for the interaction of pKal with sensor chip-immobilized 2-chain HMWK was determined by surface plasmon resonance experiments (Fig. 2B, $K_D = 72$ nM). Similar, or even higher affinity, dissociation constants (15 nM) have been previously reported for the interaction of pKal with 1-chain HMWK (47). Thus, at the physiologic HMWK concentration used in Fig. 2A (600 nM) (48) the catalytic amount of pKal present is essentially fully bound to

HMWK. As shown in Fig. 2A, DX-2930 inhibits both free and HMWK-bound pKal with equivalent K_i^{app} values. Consistent with the formation of a saturated pKal-HMWK complex, we obtained similar K_i^{app} values at higher HMWK concentrations (4.7 μ M) (data not shown).

DX-2930 also effectively targets the pKal-HMWK complex when bound to endothelial cells (Fig. 2C). Binding of pKal to HMWK has been previously shown to lead to the association of the resulting complex with endothelial cells (1). Specifically, ELISA experiments verified that biotinylated DX-2930 only interacted with HUVEC cells pre-loaded with pKal complexed with cell-bound HMWK. In contrast, C1-INH interacted poorly with similarly treated cells.

In addition to the above experiments that utilize a small peptide substrate, we further show that DX-2930 is a potent inhibitor of the pKal-mediated proteolysis of single-chain HMWK (its endogenous protein substrate). Addition of DX-2930 to pKal samples *in vitro* prevented the proteolysis of HMWK and

Antibody Inhibition of Plasma Kallikrein

the consequent release of bradykinin with an $IC_{50} = 1.3$ nM, as measured by bradykinin-specific ELISAs (Fig. 2D). This observed IC_{50} value is higher than the K_i^{app} value for DX-2930, which may be attributed to technical challenges with using an ELISA for enzyme kinetic measurements.

DX-2930 Only Inhibits Active pKal—Several findings established that DX-2930 specifically targets activated pKal, and in particular the active site of the enzyme. First, DX-2930 did not inhibit any of the 20 different serine proteases listed under “Experimental Procedures” (including the 68% identical FXIa catalytic domain) at a final concentration of 1 μ M DX-2930. Second, SPR experiments (Fig. 2E) demonstrated that DX-2930 binds active pKal, but binding is markedly diminished to an equivalent amount of prekallikrein or to pKal that has been inactivated with a small molecule, active site-directed inhibitor (AEBSF). This latter finding suggests that the antibody interacts with the pKal active site given that AEBSF covalently modifies the active site serine (49). Importantly, SDS-PAGE experiments that analyze DX-2930 samples preincubated with and without an equimolar concentration (2 μ M) of pKal demonstrate that the antibody is not cleaved (Fig. 2F).

Structure of the DX-2930-pKal Complex—To understand the interaction between DX-2930 and pKal with atomic resolution, we crystallized the Fab portion of DX-2930 both alone and in a complex with a deglycosylated variant of the human pKal catalytic domain (35). Diffraction data for Fab-only crystals (collected to 1.75 Å) and the pKal-DX-2930 Fab complex (to 2.1 and 2.4 Å for different crystal forms) was used to solve the structures by molecular replacement methods that employed the coordinates of both a generalized Fab framework without CDR loops and the pKal catalytic domain structure PDB 2ANY as the search models. Subsequent building/refinement resulted in the final complex and apo-Fab structures presented in Fig. 3, with diffraction and refinement statistics presented in Table 2. Overall, the three final complex structures (one in the asymmetric unit of PDB 4OGX and two in the asymmetric unit of PDB 4OGY) are highly similar, with small adjustments in the interface such that alignments centered on either the Fab or pKal yield lower deviations for the respective chains (Fig. 3B). Both the pKal catalytic domain (r.m.s.d. 0.36 Å, Fig. 3C) and DX-2930 Fab (r.m.s.d. 1.09 Å, Fig. 3D) that are present in the complex deviate little from their individual apo structures. However, DX-2930 heavy chain CDR loops do not have resolvable density in the apo structure.

Inspection of the complex structure reveals the reason why DX-2930 prevents substrate proteolysis by pKal. Namely, the Fab interface covers ~ 2400 Å² of surface and completely obstructs the active site of pKal (Fig. 4A). Direct contributions to this interface are made by Fab CDR and framework (FR) residues from both the heavy chain (HV-FR1, HV-CDR1, and HV-CDR3) and the light chain (LV-CDR2). Hydrophobic interactions of HV-FR1 residues, particularly Phe-27 and Phe-29, dominate the interface of this motif with pKal residues Val-410, Leu-412, Arg-416, Leu-418, Leu-439, Lys-575, and the His-434 of the pKal catalytic triad (Fig. 4B; prekallikrein numbering is used). For reference, the pKal residues His-434, Asp-483, and Ser-578 are equivalent to chymotrypsin catalytic triad residues His-57, Asp-102, and Ser-195, respectively. Moreover, His-31

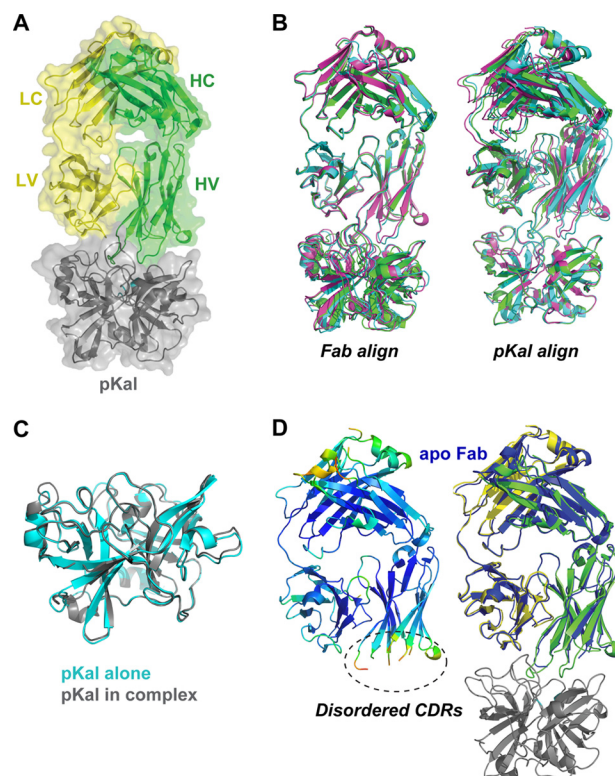


FIGURE 3. X-ray crystallographic analysis of the pKal catalytic domain complexed with the DX-2930 Fab. A, ribbon structure of the pKal-DX-2930 Fab complex (PDB 4OGX) with transparent surface rendering. pKal ribbon is colored in gray with cyan marking the catalytic triad residues, and the DX-2930 Fab is in green (heavy chain) and yellow (light chain). B, all three resolved DX-2930-pKal complex structures from this study overlaid in ribbon (orientation as in A) with alignment on the Fab domain or pKal catalytic domain. Complex from PDB 4OGX is colored in magenta, and the two distinct complexes from PDB 4OGY are in cyan and green. C, overlay of pKal catalytic domain structure alone (cyan, PDB 1ANY) with the pKal catalytic domain crystallized in complex with DX-2930 (gray, from PDB 4OGX) reveals minimal changes in the bound/unbound forms (r.m.s.d. 0.36 Å). D, left, crystal structure of the unbound DX-2930 Fab (PDB 4PUB) in ribbon with color reflecting B-factor values reveals disordered heavy chain CDR loops but an intact light chain CDR2. Right, overlay of the apo-DX-2930 Fab (now all in blue) overlaid on the pKal-DX-2930 Fab complex structure (colored as in A).

of CDR1 forms a hydrogen bond with the backbone carbonyl of pKal residue Asp-437, and it consequently flips the Asp-437–Gly-438 peptide bond relative to the apo structure of the pKal catalytic domain. On the opposite side of the complex interface, Lys-50 of LV-CDR2 makes a side chain-mediated interaction with pKal residues Tyr-555 and Glu-600 (Fig. 4C). This interface is also supported by several backbone-mediated hydrogen bonds made by pKal residues Glu-527 (contacting amide nitrogen of Gly-57), Lys-528 (contacting carbonyl oxygen of Ser-56), and Arg-604 (interacting with carbonyl oxygen atoms of Leu-54 and Glu-55).

The most intimate interactions between the DX-2930 Fab and pKal catalytic domain are mediated by the same heavy chain CDR3 residues that led to affinity improvements (Table 1). The CDR3 loop extends deeply into the active site of pKal (Fig. 4D) and interacts with both the substrate binding region and the catalytic triad. Arg-106 anchors the loop, burying into the canonical S1 binding pocket and forming a bidentate bonding interaction with pKal D572, much like the broad serine protease inhibitor benzamidine (Fig. 4, D and E). This interac-

TABLE 2
X-ray crystallographic collection and refinement statistics

| PDB ID | 4OGX | 4OGY | 4PUB |
|-----------------------------|---|---|---|
| Crystal ID | 242118h7 | 242121d10 | 243341c6 |
| Precipitant | 0.1 M imidazole, pH 6.5, 30% MPD ^a , 0.2 M (NH ₄) ₂ SO ₄ , 10% PEG 3350 | 0.1 M BisTris ^a , pH 6.5, 20% PEG 5000 MME | 0.09% BisTris, pH 5.5, 22.5% PEG 3500, 3% DMSO |
| Cryoprotectant | None | 20% ethylene glycol | None |
| Crystallization Temperature | 16 °C | 16 °C | 16 °C |
| Beam line | Rigaku FR-E+ SuperBright/Saturn 944+ CCD | Rigaku FR-E+ SuperBright/Saturn 944+ CCD | APS LS-CAT 21 ID-F |
| Space group | <i>P</i> 2 ₁ 2 ₁ 2 ₁ | <i>P</i> 2 ₁ | <i>P</i> 2 ₁ 2 ₁ 2 ₁ |
| Unit cell | <i>a</i> = 109.6, <i>b</i> = 171.5, <i>c</i> = 42.32 Å $\alpha = \beta = \gamma = 90^\circ$ | <i>a</i> = 82.12, <i>b</i> = 113.8, <i>c</i> = 89.05 Å $\alpha = \gamma = 90^\circ, \beta = 94.70^\circ$ | <i>a</i> = 45.93, <i>b</i> = 60.54, <i>c</i> = 150.49 Å $\alpha = \beta = \gamma = 90^\circ$ |
| Solvent content | 56% | 54% | 44% |
| <i>V_m</i> | 2.8 Å ³ /Da | 2.67 Å ³ /Da | 2.2 Å ³ /Da |
| Resolution | 50-2.4 Å (2.45-2.4 Å) ^b | 50-2.1 Å (2.14-2.10 Å) | 50-1.75 Å (1.79-1.75 Å) |
| <i>I</i> / σ | 15.7 (2.9) | 22.6 (5.8) | 22.4 (3.8) |
| Completeness | 99.9% (99.6%) | 99.8% (99.8%) | 99.1% (99.8%) |
| <i>R_{merge}</i> | 0.112 (0.477) | 0.076 (0.364) | 0.051 (0.471) |
| Multiplicity | 6.7 (4.0) | 7.3 (6.1) | 6.1 (6.1) |
| Reflections | 32,218 (2323) | 94,897 (6934) | 42,967 (3147) |
| Mosaicity | 0.6 | 0.3 | 0.3 |
| Refinement | | | |
| <i>R</i> | 0.188 (0.241) | 0.185 (0.202) | 0.174 (0.242) |
| <i>R_{free}</i> | 0.236 (0.296) | 0.221 (0.244) | 0.214 (0.289) |
| Validation ^c | | | |
| Ramachandran favored | 96.8% | 97.5% | 97.8% |
| Ramachandran outliers | 0.0% | 0.0% | 0.2% |
| Rotamer outliers | 1.8% | 0.8% | 1.4% |
| Clash score | 5.68 (99th percentile) | 2.71 (99th percentile) | 5.35 (94th percentile) |
| Molprobrity score | 1.71 (98th percentile) | 1.17 (100th percentile) | 1.45 (95th percentile) |

^a BisTris is 2-[bis(2-hydroxyethyl)amino]-2-(hydroxymethyl)propane-1,3-diol and MPD is 2-methyl-2,4-pentanediol.

^b Statistics for highest resolution shell data are shown in parentheses throughout the table.

^c Validation statistics were obtained from Molprobrity (79).

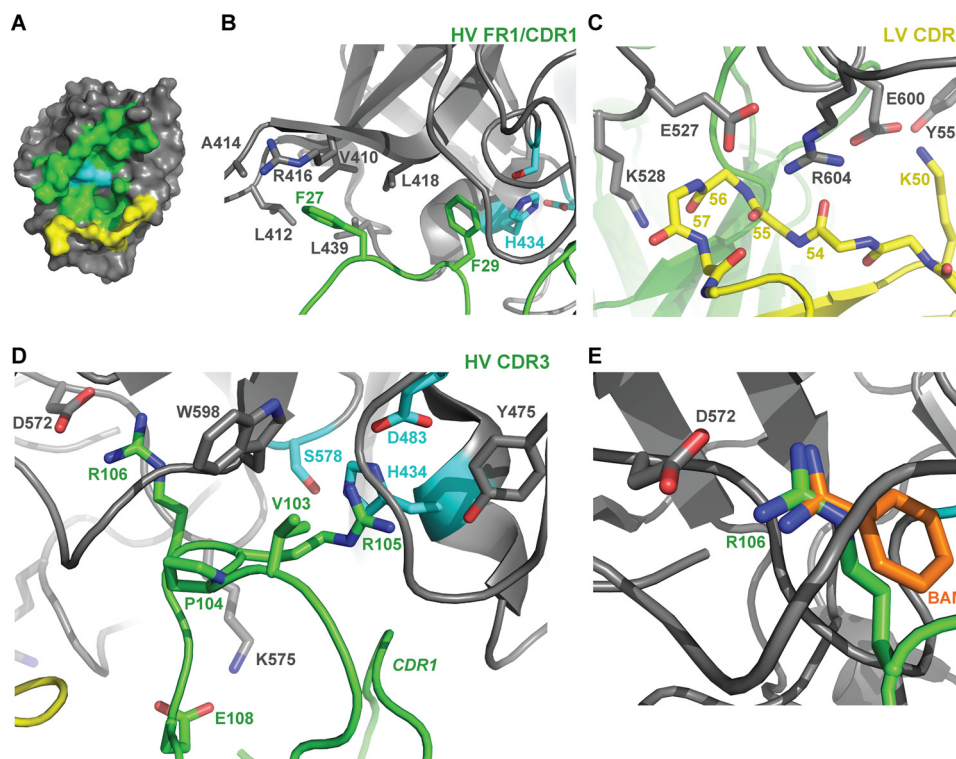


FIGURE 4. Structural analysis of DX-2930 CDR interactions with the pKal catalytic domain. *A*, surface rendering of the pKal catalytic domain highlighting complex interface residues, with heavy chain-interacting residues in green and light chain-interacting ones in yellow. Detailed views of critical side-chain interactions between pKal and the DX-2930 Fab residues are shown as follows: *B*, heavy chain FR1 and CDR1 (HV FR1/CDR1); *C*, light chain CDR2 (LV CDR2); and *D*, heavy chain CDR3 (HV CDR3). *E*, overlay of the benzamidine molecule from PDB 2ANY reveals a bidentate interaction with pKal residue Asp-572 (chymotrypsin Asp-195) in a manner analogous to Arg-106 of the DX-2930 Fab.

tion is preceded on the N-terminal side of the CDR by contacts of both Pro-104 and Arg-105, which abuts the catalytic triad, and directly bonds with Asp-483, with the S3 and S2 substrate

binding pockets of pKal, respectively. Val-103 appears to have enough hydrophobic character to interact with pKal Tyr-555 and Trp-598 but not so large that it disrupts a nearby loop in

Antibody Inhibition of Plasma Kallikrein

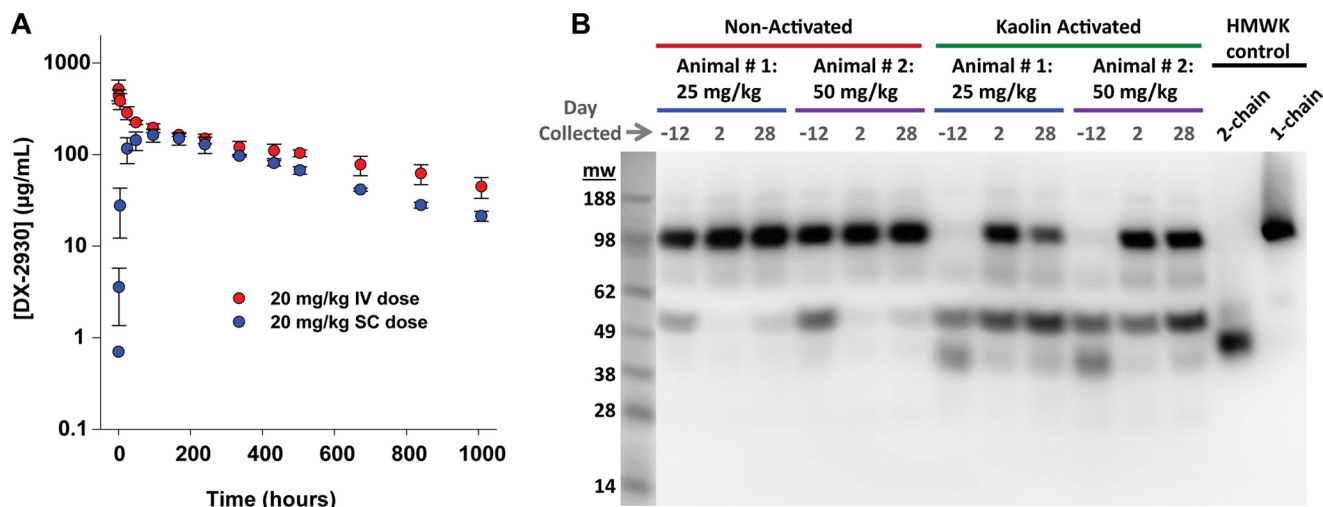


FIGURE 5. Pharmacokinetic and pharmacodynamic properties of DX-2930 in cynomolgus monkey. *A*, 20 mg/kg DX-2930 was dosed by either intraperitoneal (IP) or subcutaneous (SC) injection. Citrated plasma was collected at indicated times (hours) post-dose, and the concentration of DX-2930 was measured by a quantitative ELISA utilizing an antibody specific for DX-2930 (see “Experimental Procedures”). The s.c. dosing results in a maximal DX-2930 concentration reached by 96 h and a prolonged serum half-life of ~12.5 days. Noncompartmental pharmacokinetic analyses yield the parameters shown in Table 3. Error bars shown are the standard deviation between replicates ($n = 3$). *B*, inhibition of pKal-mediated HMWK cleavage by DX-2930 in activated plasma. The KKS in plasma collected from cynomolgus monkeys subcutaneously treated with 25 mg/kg or 50 mg/kg DX-2930 was activated by kaolin addition and samples analyzed by Western blots detecting intact 1-chain or proteolyzed 2-chain HMWK. A light image of included molecular mass standards (in kDa) is shown adjacent to the Western blot image. Purified human 1- and 2-chain HMWK at 5 nM were included as controls. Addition of DX-2930 reduces HMWK proteolysis relative to nondosed samples (day -12) even when sampled 28 days post-injection.

TABLE 3

Pharmacokinetic parameters of DX-2930 in cynomolgus monkeys

| Group | Route | C_{max} µg/ml | AUC_{last} $h \times \mu\text{g/ml}$ | CL ml/h/kg | V_{ss} ml/kg | $t_{1/2}$ h |
|-------|-------|--------------------|---|---------------|-------------------|----------------|
| 1 | i.v. | 519.7 (133.1) | 116,447.4 ^a (16463.2) | 0.14 (0.03) | 86.3 (5.6) | 463.8 (68.9) |
| 2 | s.c. | 162.8 (26.3) | 77,024.8 ^a (6252.0) | 0.23 (0.02) | NA | 301.1 (5.4) |

^a The percent bioavailability when administered by the s.c. route was approximately 66% (s.c. $AUC_{last}/i.v. AUC_{last}$), where AUC_{last} is area under the curve from time 0 to the time of last quantifiable concentration; V_{ss} is apparent volume of distribution at steady state; CL is clearance. Values in parentheses are standard errors of the mean as determined by WinNonlin noncompartmental analyses (Pharsight).

pKal (residues 478–480) that further interacts/stabilizes both HV CDR1 and CDR3. Finally, Glu-108, which is predominantly acidic/polar in the most inhibitory affinity maturation variants, contacts Lys-575 of pKal in an interaction that is likely to be a significant driver of DX-2930 specificity with respect to other serine proteases, most of which have a Gln or Glu at this position (35). Although not directly involved in pKal interactions, the CDR3 residues ⁹⁹RRIG, Asp-107, and ¹⁰⁹FDI that were also included in the affinity maturation rounds make Fab intramolecular contacts that stabilize the CDR3 loop conformation and also likely contribute to the overall folding stability of the Fab.

Taken together, the composition and extended length of the HV CDR3 allows the intimate contact of this loop with the pKal active site, while being short enough to steer the potentially labile peptide backbone of this loop away from the proteolytic residues of pKal. Of note, the complex structure is consistent with a proposed competitive inhibition mechanism given that binding of this antibody to pKal will exclude even small peptide substrates from the pKal active site.

Pharmacokinetic and Pharmacodynamic Analysis of DX-2930—To develop a long term prophylactic inhibitor of pKal, it was necessary to demonstrate a sustained bioactivity of DX-2930 *in vivo*. Toward this end, the pharmacokinetic profile of DX-2930 injected both s.c. and i.v. into cynomolgus monkeys at 20 mg/kg was examined, revealing a high bioavailability (66%) and sus-

tained half-life of ~12.5 and 19.3 days, respectively (Fig. 5A and Table 3). The injected dose of DX-2930 also retains bioactivity throughout its residence in the circulation. Specifically, plasma samples from monkeys that were dosed with or without s.c. DX-2930 were treated *ex vivo* with kaolin to activate the contact system, and the proteolytic activity of the resulting pKal was assessed by monitoring the presence or absence of cleaved 2-chain HMWK by Western blot analysis (Fig. 5B). DX-2930 inhibited the pKal-mediated proteolysis of HMWK even at 28 days following s.c. dosing, a finding consistent with the prolonged serum half-life of DX-2930.

DX-2930 Treatment Reduces Carrageenan-induced Paw Edema in Rats—To begin addressing the *in vivo* efficacy of DX-2930, we investigated the ability of DX-2930 to diminish carrageenan-induced paw edema (CPE) in rats. CPE is not a disease model of HAE but is a commonly used model of general inflammation that involves several mediators including pro-inflammatory cytokines, histamine, 5-hydroxytryptamine, and prostaglandins, in addition to kinins (50, 51). Rats were pretreated with s.c. DX-2930 24 h prior to the injection of 1% carrageenan into the right hind paw to induce edema, and dose-dependent reductions in swelling were recorded (Fig. 6). DX-2930 (30 mg/kg) reduced paw edema at 8 h by 55.6% compared to vehicle-treated rats. The COX inhibitor indomethacin was used as a positive control and reduced paw edema at 8 h by

47.2% compared with vehicle. Full inhibition is not reached by either inhibitor as expected given that multiple parallel inflammatory pathways cause CPE. However, the significant reduction in CPE with both DX-2930 and indomethacin treatment

does demonstrate the inhibition of kinin-mediated prostaglandin biosynthesis in this model. Furthermore, the efficacy of DX-2930 24 h after subcutaneous dosing demonstrates the potential for this antibody in prophylactic KKS inhibition.

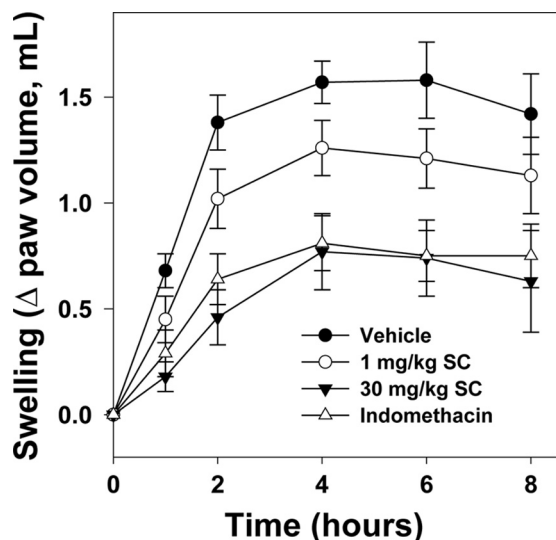


FIGURE 6. DX-2930 inhibits carrageenan-induced paw edema in the rat. DX-2930 was administered via a s.c. injection 24 h prior to carrageenan injection into the rat hind paw, although the vehicle (Formulation Buffer) and indomethacin (5 mg/kg) controls were administered by i.p. injection 30 min prior to carrageenan treatment. Paw volume was measured at the indicated time points following carrageenan injection and averaged for each treatment group ($n = 10$). Error calculated using the standard deviation.

DISCUSSION

Dysregulated contact system activation is central to the pathophysiology of HAE, and HAE attacks can be effectively treated with inhibitors that either prevent pKal-mediated proteolytic production of bradykinin or antagonize the B2 receptor. We used phage display to select and develop a potent, specific, and long-lived antibody inhibitor of pKal, DX-2930. X-ray crystallographic analysis of the DX-2930 Fab region bound to pKal details the molecular basis of our discovery, demonstrating that the antibody binds and occludes the substrate-binding active site region of the protease.

The DX-2930 mechanism of inhibition is similar to that employed by other well described serine protease inhibitors. For instance, amino acid Arg-106 of DX-2930 HV-CDR3 buries deeply into the canonical S1 substrate binding pocket in a manner similar to both benzamidine (Fig. 4, *D* and *E*, and Fig. 7*A*) and the lysine side chain of the broad specificity inhibitor BPTI/aprotinin (Fig. 7*B*). With respect to reported antibody inhibitors of serine proteases, Craik and co-workers (52) characterized three antibodies that bind matriptase (MT-SP1) whereby the interacting HV-CDR3 residues align in a C-terminal to N-terminal orientation rather than the substrate-like N-termi-

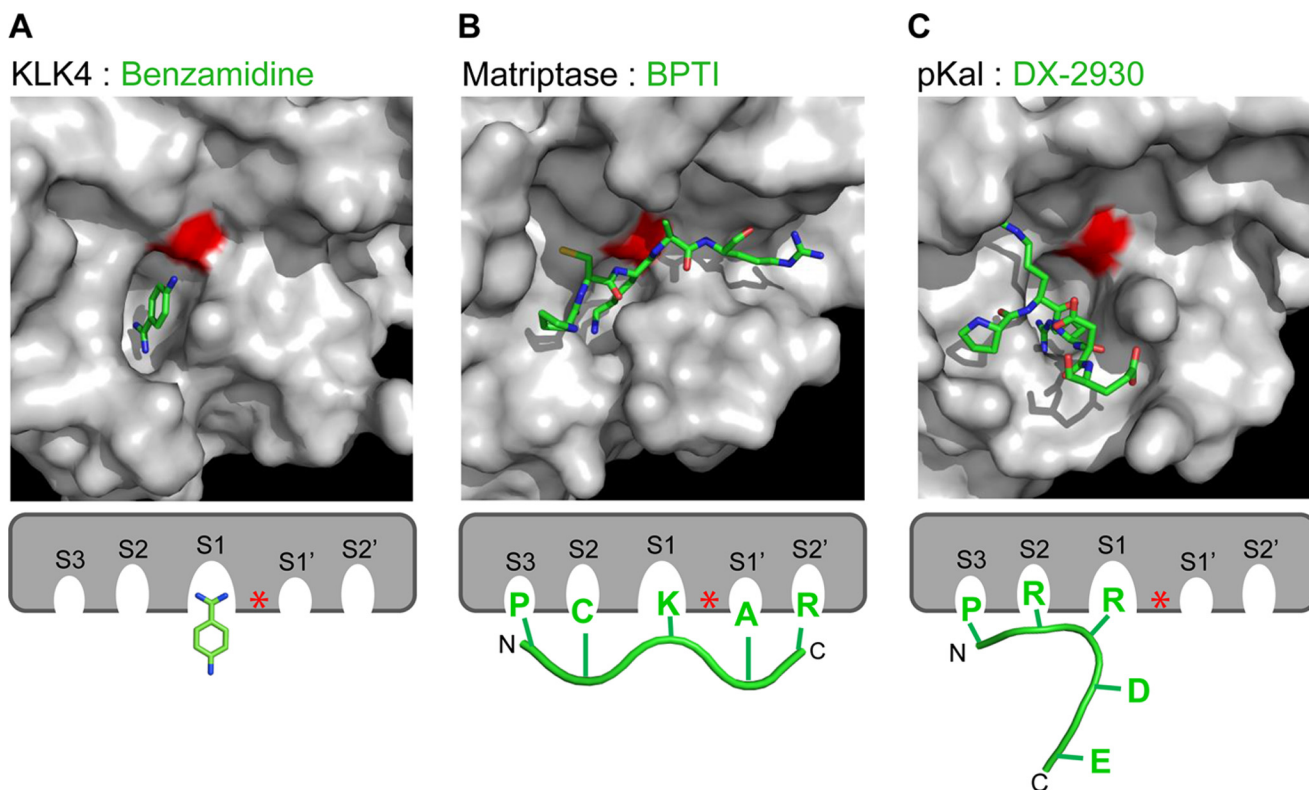


FIGURE 7. Comparison of inhibitor interactions with serine protease active site pockets. Surface rendering of serine proteases are shown docked with stick models of their respective ligands just above the schematic models of these interactions with canonical protease docking sites highlighted. *A*, small molecule benzamidine docks into the deep S1 binding pocket of KLK4 (PDB 2BDG). *B*, peptide sequence from the small protein BPTI binds matriptase in a "substrate-like" mode (PDB 1EAW). *C*, part of the HV-CDR3 of DX-2930 binds the S1-S3 sites of pKal and then abruptly turns away from the catalytic serine. *N* and *C* refer to N- and C-terminal ends of docked schematic peptides. Inhibitor stick color scheme by atom: blue, nitrogen; red, oxygen; green, carbon. Red in surface representation and red asterisk in schematic representation denote the catalytic serine residue.

Antibody Inhibition of Plasma Kallikrein

nal to C-terminal orientation (e.g. BPTI in Fig. 7B). This reverse orientation allows the antibodies to bind the scission machinery of an active protease without resulting in their proteolysis. In contrast, DX-2930 binds in the substrate-like N-terminal to C-terminal orientation in the S1-S3 subsites, even to the extent that it chemically and structurally mimics the P3 proline and P1 arginine present in the natural pK_{al} substrate, HMWK. However, the orientation of the HV-CDR3 loop in DX-2930 prevents interactions with subsites S1'-S3', and thereby it prevents its cleavage by the pK_{al} catalytic serine (Fig. 7C). Importantly from the perspective of an antibody therapeutic, we demonstrate that DX-2930 is indeed not proteolyzed by pK_{al} (Fig. 2F) despite such an intimate complex formation.

The crystal structure of prekallikrein is not available, but the likely structural homology to the related proenzyme form of kallikrein 6, whose crystal structure has been defined (53), suggests that the S1 pocket (and other active site residue conformations) would only be present in the activated pK_{al} form and not in prekallikrein. Thus, given the significant contact of DX-2930 HV-CDR3 residues with the pK_{al} active site, it is not surprising that our SPR binding studies (Fig. 2E) demonstrate that DX-2930 does not bind prekallikrein.

A lack of prekallikrein binding was an intentional primary selection criterion to potentially reduce the therapeutic levels of DX-2930 necessary to inhibit pK_{al} activity. Prekallikrein is present in plasma at a concentration of ~500 nM, and we reasoned that binding to prekallikrein would necessitate drug levels at equivalent concentrations. In contrast, a potent antibody inhibitor that bound only the active form of the enzyme could be dosed to levels that match the amount of pK_{al} generated in disease. pK_{al} levels between 30 and 110 nM have been estimated in HAE plasma, and an effective dose of ecallantide for the treatment of acute attacks of HAE has a C_{max} of ~80 nM (586 ng/ml) (54, 55). Therapeutic pK_{al} inhibition has the potential to attenuate kinin production, as well as to limit the formation of active pK_{al} generated by the cyclical pK_{al}-mediated conversion of FXII to FXIIa. Therefore, it is possible that prophylactic inhibition of pK_{al} activity may require a lower dose of inhibitor than that needed to acutely treat an HAE attack. However, future clinical studies in HAE will help elucidate the DX-2930 dose necessary for successful long term attack prophylaxis.

Certain properties of DX-2930 may support its use as a novel reagent to investigate contact system activation in biological systems or as a potential therapy for the treatment of pK_{al}-mediated diseases, such as HAE. First, the specificity of DX-2930 toward binding activated pK_{al}, rather than prekallikrein or any other tested serine protease suggests that it could prove to be a useful reagent to detect biological sites where active pK_{al} is generated. Second, DX-2930 can target free soluble pK_{al}, as well as pK_{al} complexed with HMWK that may be further associated with endothelial cells (Fig. 2, A–C). In contrast, pK_{al} is resistant to inhibition by endogenous inhibitors C1-INH and α 2-macroglobulin (α 2M) when it is bound to HMWK on endothelial cells, a property it shares with other cell-bound proteases such as plasmin and urokinase-type plasminogen activator (56, 57). Such observations support the concept that HAE attack localization may be partially attributed to endothelial cell-bound pK_{al}. Third, our studies in non-human

primates demonstrate that DX-2930 has a long pharmacokinetic half-life (12.5 days in non-human primates, Fig. 5A and Table 3). Our recent completion of a phase 1A clinical study further reveals that DX-2930 has an almost 3-week half-life in healthy human individuals (58). Finally, DX-2930 exhibits striking specificity for pK_{al}, which differs from the endogenous C1-INH, which has likely evolved to target numerous serine proteases and has been reported to inhibit 12 of the 20 human serine proteases that were tested in this study (59–69). Taken together, high therapeutic doses of C1-INH are likely required for the treatment of HAE to offset its limited potency and broad specificity and may account for the occurrence of breakthrough attacks with current prophylactic approaches (70).

Contact system activation is observed in a variety of diseases associated with the hallmarks of inflammation (heat, redness, pain, and swelling) (1), implying that the activation and regulation of the contact system is tightly controlled in normal physiology. Here, we demonstrate using DX-2930-treated rats that plasma kallikrein is a mediator in CPE. Although not a specific disease model of HAE, bradykinin is one of several mediators in CPE (51), and the observed efficacy of DX-2930 in this model supports its on-target *in vivo* bioactivity. As a highly specific pK_{al} inhibitor with *in vivo* efficacy, DX-2930 can be used to investigate the therapeutic benefit of pK_{al} inhibition in other diseases reported to have elevated contact system activation. The role of the plasma KKS system in thrombosis has been particularly intriguing given that the targeted disruption of contact system proteins appears to reduce thrombus formation without increasing bleeding in animal models of venous and arterial thrombosis (71–77).

Interestingly, for such a conserved biological system, a genetic deficiency in prekallikrein or other contact system proteins (FXII and HMWK) is not associated with disease, including risk for bleeding, which suggests that chronic pK_{al} inhibition could be well tolerated (78). Combining its potency with expected long half-life in patient circulation, DX-2930 may prove to be an effective prophylactic treatment of chronic diseases mediated by contact system activation, including HAE.

Acknowledgments—We thank Joe Biedenkapp (Dyax Corp.) for help in the preparation of this manuscript and scientific services provided by Cell Technology Inc. (Mountain View, CA), Reaction Biology (Malvern, PA), WIL Research (Ashland, OH), and Washington Biotechnology (Baltimore, MD).

REFERENCES

1. Colman, R. W., and Schmaier, A. H. (1997) Contact system: a vascular biology modulator with anticoagulant, profibrinolytic, antiadhesive, and proinflammatory attributes. *Blood* **90**, 3819–3843
2. Leeb-Lundberg, L. M., Marceau, F., Müller-Esterl, W., Pettibone, D. J., and Zuraw, B. L. (2005) International union of pharmacology. XLV. Classification of the kinin receptor family: from molecular mechanisms to pathophysiological consequences. *Pharmacol. Rev.* **57**, 27–77
3. Oschatz, C., Maas, C., Lecher, B., Jansen, T., Björkqvist, J., Tradler, T., Sedlmeier, R., Burfeind, P., Cichon, S., Hammerschmidt, S., Müller-Esterl, W., Wuillemin, W. A., Nilsson, G., and Renné, T. (2011) Mast cells increase vascular permeability by heparin-initiated bradykinin formation *in vivo*. *Immunity* **34**, 258–268
4. Maas, C., Govers-Riemslog, J. W., Bouma, B., Schiks, B., Hazenberg, B. P.,

- Lokhorst, H. M., Hammarström, P., ten Cate, H., de Groot, P. G., Bouma, B. N., and Gebbink, M. F. (2008) Misfolded proteins activate factor XII in humans, leading to kallikrein formation without initiating coagulation. *J. Clin. Invest.* **118**, 3208–3218
5. van der Meijden, P. E., Munnix, I. C., Auger, J. M., Govers-Riemslog, J. W., Cosemans, J. M., Kuijpers, M. J., Spronk, H. M., Watson, S. P., Renné, T., and Heemskerk, J. W. (2009) Dual role of collagen in factor XII-dependent thrombus formation. *Blood* **114**, 881–890
 6. Schousboe, I., and Nyström, B. (2009) High molecular weight kininogen binds to laminin—characterization and kinetic analysis. *FEBS J.* **276**, 5228–5238
 7. White-Adams, T. C., Berny, M. A., Patel, I. A., Tucker, E. I., Gailani, D., Gruber, A., and McCarty, O. J. (2010) Laminin promotes coagulation and thrombus formation in a factor XII-dependent manner. *J. Thromb. Haemost.* **8**, 1295–1301
 8. Kannemeier, C., Shibamiya, A., Nakazawa, F., Trusheim, H., Ruppert, C., Markart, P., Song, Y., Tzima, E., Kennerknecht, E., Niepmann, M., von Bruehl, M. L., Sedding, D., Massberg, S., Günther, A., Engelmann, B., and Preissner, K. T. (2007) Extracellular RNA constitutes a natural procoagulant cofactor in blood coagulation. *Proc. Natl. Acad. Sci. U.S.A.* **104**, 6388–6393
 9. Smith, S. A., Mutch, N. J., Baskar, D., Rohloff, P., Docampo, R., and Morrissey, J. H. (2006) Polyphosphate modulates blood coagulation and fibrinolysis. *Proc. Natl. Acad. Sci. U.S.A.* **103**, 903–908
 10. Müller, F., Mutch, N. J., Schenk, W. A., Smith, S. A., Esterl, L., Spronk, H. M., Schmidbauer, S., Gahl, W. A., Morrissey, J. H., and Renné, T. (2009) Platelet polyphosphates are proinflammatory and procoagulant mediators *in vivo*. *Cell* **139**, 1143–1156
 11. Sanchez, J., Elgue, G., Larsson, R., Nilsson, B., and Olsson, P. (2008) Surface-adsorbed fibrinogen and fibrin may activate the contact activation system. *Thromb. Res.* **122**, 257–263
 12. Tapper, H., and Herwald, H. (2000) Modulation of hemostatic mechanisms in bacterial infectious diseases. *Blood* **96**, 2329–2337
 13. Nielsen, V. G., Steenwyk, B. L., and Gurley, W. Q. (2006) Contact activation prolongs clot lysis time in human plasma: role of thrombin-activatable fibrinolysis inhibitor and Factor XIII. *J. Heart Lung Transplant.* **25**, 1247–1252
 14. Rahman, M. M., Bhoola, K. D., Elson, C. J., Lemon, M., and Dieppe, P. A. (1995) Identification and functional importance of plasma kallikrein in the synovial fluids of patients with rheumatoid, psoriatic, and osteoarthritis. *Ann. Rheum. Dis.* **54**, 345–350
 15. Stadnicki, A., Gonciarz, M., Niewiarowski, T. J., Hartleb, J., Rudnicki, M., Merrell, N. B., Dela Cadena, R. A., and Colman, R. W. (1997) Activation of plasma contact and coagulation systems and neutrophils in the active phase of ulcerative colitis. *Dig. Dis. Sci.* **42**, 2356–2366
 16. Weiser, P., Qian, Y., Pan, J., Zhou, X., Lu, H., Studelska, D. R., Shih, F. F., and Zhang, L. (2010) Activated contact system and abnormal glycosaminoglycans in lupus and other auto- and non-autoimmune diseases. *Prog. Mol. Biol. Transl. Sci.* **93**, 443–472
 17. Phipps, J. A., and Feener, E. P. (2008) The kallikrein-kinin system in diabetic retinopathy: lessons for the kidney. *Kidney Int.* **73**, 1114–1119
 18. Clermont, A., Chilcote, T. J., Kita, T., Liu, J., Riva, P., Sinha, S., and Feener, E. P. (2011) Plasma kallikrein mediates retinal vascular dysfunction and induces retinal thickening in diabetic rats. *Diabetes* **60**, 1590–1598
 19. Coppola, R., Cristilli, P., Cugno, M., Ariens, R. A., Mari, D., and Mannucci, P. M. (1996) Measurement of activated factor XII in health and disease. *Blood Coagul. Fibrinolysis* **7**, 530–535
 20. Miller, R. L., Verma, P. S., and Adams, R. G. (1983) Studies of the kallikrein-kinin system in patients with sickle cell anemia. *J. Natl. Med. Assoc.* **75**, 551–556
 21. Bergamaschini, L., Donarini, C., Gobbo, G., Parnetti, L., and Gallai, V. (2001) Activation of complement and contact system in Alzheimer's disease. *Mech. Ageing Dev.* **122**, 1971–1983
 22. Makevina, L. G., Lomova, I. P., Zubkov YuN., and Semenyutin, V. B. (1994) Kininogen consumption in cerebral circulation of humans during brain ischemia and postischemic reperfusion. *Braz. J. Med. Biol. Res.* **27**, 1955–1963
 23. Cugno, M., Salerno, F., Mandelli, M., Lorenzano, E., Paonessa, R., and Agostoni, A. (1995) Cleavage of high molecular weight kininogen in ascites and plasma of patients with cirrhosis. *Thromb. Res.* **78**, 277–282
 24. Kaufman, N., Page, J. D., Pixley, R. A., Schein, R., Schmaier, A. H., and Colman, R. W. (1991) α 2-Macroglobulin-kallikrein complexes detect contact system activation in hereditary angioedema and human sepsis. *Blood* **77**, 2660–2667
 25. Cugno, M., Cicardi, M., Bottasso, B., Coppola, R., Paonessa, R., Mannucci, P. M., and Agostoni, A. (1997) Activation of the coagulation cascade in C1-inhibitor deficiencies. *Blood* **89**, 3213–3218
 26. Berrettini, M., Lämmle, B., White, T., Heeb, M. J., Schwarz, H. P., Zuraw, B., Curd, J., and Griffin, J. H. (1986) Detection of *in vitro* and *in vivo* cleavage of high molecular weight kininogen in human plasma by immunoblotting with monoclonal antibodies. *Blood* **68**, 455–462
 27. Bork, K., Meng, G., Staubach, P., and Hardt, J. (2006) Hereditary angioedema: new findings concerning symptoms, affected organs, and course. *Am. J. Med.* **119**, 267–274
 28. Bork, K. (2010) Diagnosis and treatment of hereditary angioedema with normal C1 inhibitor. *Allergy Asthma Clin. Immunol.* **6**, 15
 29. Caliezi, C., Wuillemin, W. A., Zeerleder, S., Redondo, M., Eisele, B., and Hack, C. E. (2000) C1-esterase inhibitor: an anti-inflammatory agent and its potential use in the treatment of diseases other than hereditary angioedema. *Pharmacol. Rev.* **52**, 91–112
 30. Bork, K. (2012) Current management options for hereditary angioedema. *Curr. Allergy Asthma Rep.* **12**, 273–280
 31. Gandhi, P. K., Gentry, W. M., and Botorff, M. B. (2012) Thrombotic events associated with C1 esterase inhibitor products in patients with hereditary angioedema: investigation from the United States Food and Drug Administration adverse event reporting system database. *Pharmacotherapy* **32**, 902–909
 32. Bork, K., Bygum, A., and Hardt, J. (2008) Benefits and risks of danazol in hereditary angioedema: a long-term survey of 118 patients. *Ann. Allergy Asthma Immunol.* **100**, 153–161
 33. Banerji, A., Sloane, D. E., and Sheffer, A. L. (2008) Hereditary angioedema: a current state-of-the-art review, V: attenuated androgens for the treatment of hereditary angioedema. *Ann. Allergy Asthma Immunol.* **100**, S19–S22
 34. Zuraw, B. L., Busse, P. J., White, M., Jacobs, J., Lumry, W., Baker, J., Craig, T., Grant, J. A., Hurewitz, D., Bielory, L., Cartwright, W. E., Koleilat, M., Ryan, W., Schaefer, O., Manning, M., Patel, P., Bernstein, J. A., Friedman, R. A., Wilkinson, R., Tanner, D., Kohler, G., Gunther, G., Levy, R., McClellan, J., Redhead, J., Guss, D., Heyman, E., Blumenstein, B. A., Kalfus, I., and Frank, M. M. (2010) Nanofiltered C1 inhibitor concentrate for treatment of hereditary angioedema. *N. Engl. J. Med.* **363**, 513–522
 35. Tang, J., Yu, C. L., Williams, S. R., Springman, E., Jeffery, D., Sprengeler, P. A., Estevez, A., Sampang, J., Shrader, W., Spencer, J., Young, W., McGrath, M., and Katz, B. A. (2005) Expression, crystallization, and three-dimensional structure of the catalytic domain of human plasma kallikrein. *J. Biol. Chem.* **280**, 41077–41089
 36. Hekim, C., Leinonen, J., Närkänen, A., Koistinen, H., Zhu, L., Koivunen, E., Väisänen, V., and Stenman, U. H. (2006) Novel peptide inhibitors of human kallikrein 2. *J. Biol. Chem.* **281**, 12555–12560
 37. Hoet, R. M., Cohen, E. H., Kent, R. B., Rookey, K., Schoonbroodt, S., Horgan, S., Rem, L., Frans, N., Daukandt, M., Pieters, H., van Hegelsom, R., Neer, N. C., Nastri, H. G., Rondon, I. J., Leeds, J. A., Hufton, S. E., Huang, L., Kashin, I., Devlin, M., Kuang, G., Steukers, M., Viswanathan, M., Nixon, A. E., Sexton, D. J., Hoogenboom, H. R., and Ladner, R. C. (2005) Generation of high-affinity human antibodies by combining donor-derived and synthetic complementarity-determining-region diversity. *Nat. Biotechnol.* **23**, 344–348
 38. Wassaf, D., Kuang, G., Kopacz, K., Wu, Q. L., Nguyen, Q., Toews, M., Cosic, J., Jacques, J., Wiltshire, S., Lambert, J., Pazmany, C. C., Horgan, S., Ladner, R. C., Nixon, A. E., and Sexton, D. J. (2006) High-throughput affinity ranking of antibodies using surface plasmon resonance microarrays. *Anal. Biochem.* **351**, 241–253
 39. Jostock, T., Vanhove, M., Brepoels, E., Van Gool, R., Daukandt, M., Wehnert, A., Van Hegelsom, R., Dransfield, D., Sexton, D., Devlin, M., Ley, A., Hoogenboom, H., and Müllberg, J. (2004) Rapid generation of functional human IgG antibodies derived from Fab-on-phage display libraries. *J. Im-*

Antibody Inhibition of Plasma Kallikrein

- munol. Methods.* **289**, 65–80
40. Sexton, D. J., Chen, T., Martik, D., Kuzmic, P., Kuang, G., Chen, J., Nixon, A. E., Zuraw, B. L., Forteza, R. M., Abraham, W. M., and Wood, C. R. (2009) Specific inhibition of tissue kallikrein 1 with a human monoclonal antibody reveals a potential role in airway diseases. *Biochem. J.* **422**, 383–392
 41. Cha, S. (1975) Tight-binding inhibitors. I. Kinetic behavior. *Biochem. Pharmacol.* **24**, 2177–2185
 42. Morrison, J. F. (1969) Kinetics of the reversible inhibition of enzyme-catalysed reactions by tight-binding inhibitors. *Biochim. Biophys. Acta* **185**, 269–286
 43. Kuzmic, P., Elrod, K. C., Cregar, L. M., Sideris, S., Rai, R., and Janc, J. W. (2000) High-throughput screening of enzyme inhibitors: Simultaneous determination of tight-binding inhibition constants and enzyme concentration. *Anal. Biochem.* **286**, 45–50
 44. Emsley, P., and Cowtan, K. (2004) Coot: model-building tools for molecular graphics. *Acta Crystallogr. D. Biol. Crystallogr.* **60**, 2126–2132
 45. Collaborative Computational Project No. 4 (1994) The CCP4 suite: programs for protein crystallography. *Acta Crystallogr. D. Biol. Crystallogr.* **50**, 760–763
 46. Murshudov, G. N., Vagin, A. A., and Dodson, E. J. (1997) Refinement of macromolecular structures by the maximum-likelihood method. *Acta Crystallogr. D. Biol. Crystallogr.* **53**, 240–255
 47. Bock, P. E., Shore, J. D., Tans, G., and Griffin, J. H. (1985) Protein-protein interactions in contact activation of blood coagulation. Binding of high molecular weight kininogen and the 5-(iodoacetamido) fluorescein-labeled kininogen light chain to prekallikrein, kallikrein, and theseparated kallikrein heavy and light chains. *J. Biol. Chem.* **260**, 12434–12443
 48. Silverberg, M., Reddigari, S. R., and Kaplan, A. P. (1995) In *Blood: Principles and Practice of Hematology* (Handin, R. T., Lux, S. E., and Stossel, T. P., eds) pp. 1127–1150, Lippincott Williams & Wilkins, Philadelphia
 49. Markwardt, F., Drawert, J., and Walsmann, P. (1974) Synthetic low molecular weight inhibitors of serum kallikrein. *Biochem. Pharmacol.* **23**, 2247–2256
 50. Wirth, K. J., Alpermann, H. G., Satoh, R., and Inazu, M. (1992) The bradykinin antagonist Hoe 140 inhibits carrageenan- and thermally induced paw oedema in rats. *Agents Actions* **38**, 428–431
 51. Morris, C. J. (2003) Carrageenan-induced paw edema in the rat and mouse. *Methods Mol. Biol.* **225**, 115–121
 52. Schneider, E. L., Lee, M. S., Baharuddin, A., Goetz, D. H., Farady, C. J., Ward, M., Wang, C. I., and Craik, C. S. (2012) A reverse binding motif that contributes to specific protease inhibition by antibodies. *J. Mol. Biol.* **415**, 699–715
 53. Gomis-Rüth, F. X., Bayés, A., Sotiropoulou, G., Pampalakis, G., Tsetsenis, T., Villegas, V., Avilés, F. X., and Coll, M. (2002) The structure of human prokallikrein 6 reveals a novel activation mechanism for the kallikrein family. *J. Biol. Chem.* **277**, 27273–27281
 54. Stolz, L. E., and Sheffer, A. L. (2012) Prospective, double-blind, placebo-controlled trials of ecallantide for acute attacks of hereditary angioedema. *Expert Rev. Clin. Immunol.* **8**, 25–32
 55. Bernstein, J. A., and Qazi, M. (2010) Ecallantide: its pharmacology, pharmacokinetics, clinical efficacy and tolerability. *Expert Rev. Clin. Immunol.* **6**, 29–39
 56. Stephens, R. W., Pöllänen, J., Tapiovaara, H., Woodrow, G., and Vaheri, A. (1991) Stimulation of cell surface plasminogen activation by heparin and related polyionic substances. *Semin. Thromb. Hemost.* **17**, 201–209
 57. Hall, S. W., Humphries, J. E., and Gonias, S. L. (1991) Inhibition of cell surface receptor-bound plasmin by α 2-antiplasmin and α 2-macroglobulin. *J. Biol. Chem.* **266**, 12329–12336
 58. Chyung, Y., Vince, B., Iarrobino, R., Sexton, D., Kenniston, J., Faucette, R., TenHoor, C., Stolz, L. E., Stevens, C., Biedenkapp, J., and Adelman, B. (2014) A Phase 1 study to assess the safety, tolerability, pharmacokinetics and pharmacodynamics of DX-2930, a human antibody inhibitor of plasma kallikrein under investigation for long-term prophylaxis of hereditary angioedema. *Ann. Allergy Asthma Immunol.* 10.1016/j.anai.2014.05.028
 59. Marlar, R. A., Kressin, D. C., and Madden, R. M. (1993) Contribution of plasma proteinase inhibitors to the regulation of activated protein C in plasma. *Thromb. Haemost.* **69**, 16–20
 60. Nilsson, T., and Wiman, B. (1983) Kinetics of the reaction between human C1-esterase inhibitor and C1r or C1s. *Eur. J. Biochem.* **129**, 663–667
 61. Wuillemin, W. A., Eldering, E., Citarella, F., de Ruig, C. P., ten Cate, H., and Hack, C. E. (1996) Modulation of contact system proteases by glycosaminoglycans. Selective enhancement of the inhibition of factor XIa. *J. Biol. Chem.* **271**, 12913–12918
 62. Pixley, R. A., Schapira, M., and Colman, R. W. (1985) The regulation of human factor XIIa by plasma proteinase inhibitors. *J. Biol. Chem.* **260**, 1723–1729
 63. Brown, E. W., Ravindran, S., and Patston, P. A. (2002) The reaction between plasmin and C1-inhibitor results in plasmin inhibition by the serpin mechanism. *Blood Coagul. Fibrinolysis* **13**, 711–714
 64. Cugno, M., Bos, I., Lubbers, Y., Hack, C. E., and Agostoni, A. (2001) *In vitro* interaction of C1-inhibitor with thrombin. *Blood Coagul. Fibrinolysis* **12**, 253–260
 65. Heeb, M. J., and España, F. (1998) α 2-Macroglobulin and C1-inactivator are plasma inhibitors of human glandular kallikrein. *Blood Cells Mol. Dis.* **24**, 412–419
 66. Goettig, P., Magdolen, V., and Brandstetter, H. (2010) Natural and synthetic inhibitors of kallikrein-related peptidases (KLKs). *Biochimie* **92**, 1546–1567
 67. Memari, N., Jiang, W., Diamandis, E. P., and Luo, L. Y. (2007) Enzymatic properties of human kallikrein-related peptidase 12 (KLK12). *Biol. Chem.* **388**, 427–435
 68. Sulikowski, T., and Patston, P. A. (2001) The inhibition of TNK-t-PA by C1-inhibitor. *Blood Coagul. Fibrinolysis* **12**, 75–77
 69. Kruihof, E. K., Tran-Thang, C., Ransijn, A., and Bachmann, F. (1984) Demonstration of a fast-acting inhibitor of plasminogen activators in human plasma. *Blood* **64**, 907–913
 70. Porebski, G., Reshef, A., and Moldovan, D. (2013) The prophylaxis of hereditary angioedema attacks with recombinant human C1 inhibitor: who will take advantage of the individualized treatment approach? *Allergy* **68**, 1207–1209
 71. Woodruff, R. S., Xu, Y., Layzer, J., Wu, W., Ogletree, M. L., and Sullenger, B. A. (2013) Inhibiting the intrinsic pathway of coagulation with a factor XII-targeting RNA aptamer. *J. Thromb. Haemost.* **11**, 1364–1373
 72. Woodruff, R. S., Sullenger, B., and Becker, R. C. (2011) The many faces of the contact pathway and their role in thrombosis. *J. Thromb. Thrombolysis* **32**, 9–20
 73. Bird, J. E., Smith, P. L., Wang, X., Schumacher, W. A., Barbera, F., Revelli, J. P., and Seiffert, D. (2012) Effects of plasma kallikrein deficiency on haemostasis and thrombosis in mice: murine ortholog of the Fletcher trait. *Thromb. Haemost.* **107**, 1141–1150
 74. Renné, T., and Gruber, A. (2012) Plasma kallikrein: novel functions for an old protease. *Thromb. Haemost.* **107**, 1012–1013
 75. Revenko, A. S., Gao, D., Crosby, J. R., Bhattacharjee, G., Zhao, C., May, C., Gailani, D., Monia, B. P., and MacLeod, A. R. (2011) Selective depletion of plasma prekallikrein or coagulation factor XII inhibits thrombosis in mice without increased risk of bleeding. *Blood* **118**, 5302–5311
 76. Crosby, J. R., Marzec, U., Revenko, A. S., Zhao, C., Gao, D., Matafonov, A., Gailani, D., MacLeod, A. R., Tucker, E. I., Gruber, A., Hanson, S. R., and Monia, B. P. (2013) Antithrombotic effect of antisense factor XI oligonucleotide treatment in primates. *Arterioscler. Thromb. Vasc. Biol.* **33**, 1670–1678
 77. Langhauser, F., Göb, E., Kraft, P., Geis, C., Schmitt, J., Brede, M., Göbel, K., Helluy, X., Pham, M., Bendszus, M., Jakob, P., Stoll, G., Meuth, S. G., Nieswandt, B., McCrae, K. R., and Kleinschnitz, C. (2012) Kininogen deficiency protects from ischemic neurodegeneration in mice by reducing thrombosis, blood-brain barrier damage, and inflammation. *Blood* **120**, 4082–4092
 78. Girolami, A., Scarpato, P., Candeo, N., and Lombardi, A. M. (2010) Congenital prekallikrein deficiency. *Expert Rev. Hematol.* **3**, 685–695
 79. Chen, V. B., Arendall, W. B., 3rd, Headd, J. J., Keedy, D. A., Immormino, R. M., Kapral, G. J., Murray, L. W., Richardson, J. S., and Richardson, D. C. (2010) MolProbity: all-atom structure validation for macromolecular crystallography. *Acta Crystallogr. D. Biol. Crystallogr.* **66**, 12–21